

# Functional interlayer of PVDF-HFP and carbon nanofiber for long-life lithium-sulfur batteries

Anyi Zhang<sup>1,§</sup>, Xin Fang<sup>1,§</sup>, Chenfei Shen<sup>1</sup>, Yihang Liu<sup>2</sup>, In Gi Seo<sup>1</sup>, Yuqiang Ma<sup>3</sup>, Liang Chen<sup>2</sup>, Patrick Cottingham<sup>4</sup>, and Chongwu Zhou<sup>2</sup> (✉)

<sup>1</sup> Mork Family Department of Chemical Engineering and Materials Science, University of Southern California, Los Angeles, California 90089, USA

<sup>2</sup> Ming Hsieh Department of Electrical Engineering, University of Southern California, Los Angeles, California 90089, USA

<sup>3</sup> Department of Physics and Astronomy, University of Southern California, Los Angeles, California 90089, USA

<sup>4</sup> Department of Chemistry, University of Southern California, Los Angeles, California 90089, USA

<sup>§</sup> Anyi Zhang and Xin Fang contributed equally in this work

**Received:** 18 September 2017

**Revised:** 8 November 2017

**Accepted:** 20 November 2017

© Tsinghua University Press  
and Springer-Verlag GmbH  
Germany, part of Springer  
Nature 2017

## KEYWORDS

lithium-sulfur batteries,  
PVDF-HFP,  
gel polymer electrolyte,  
carbon nanofiber,  
conductive network

## ABSTRACT

In the present work, we develop a scalable and inexpensive design for lithium-sulfur (Li-S) batteries by capping a flexible gel polymer/carbon nanofiber (CNF) composite membrane onto a free-standing and binder-free CNF + Li<sub>2</sub>S<sub>8</sub> cathode, thus achieving a three-dimensional (3D) structural design. The CNF network is used as the current collector and S holder to overcome the insulating nature and volume expansion of S, while the composite membrane comprises a gel polymer poly(vinylidene fluoride-co-hexafluoropropylene) (PVDF-HFP), and CNF additive is used as an interlayer to trap polysulfides and recycle the remaining S species, leading to a high specific capacity and long cycle life. This 3D structure enables excellent cyclability for 500 cycles at 0.5 °C with a small capacity decay of 0.092% per cycle. Furthermore, an outstanding cycle stability was also achieved at even higher current densities (1.0 to 2.0 °C), indicating its good potential for practical applications of Li-S batteries.

## 1 Introduction

With the increased popularity of portable electronic devices and electric vehicles, there is a demand for enhanced lithium-ion battery (LIB) performance. However, the theoretical specific capacities of commercial cathode materials, such as LiCoO<sub>2</sub> (274 mAh·g<sup>-1</sup>) [1] and LiFePO<sub>4</sub> (170 mAh·g<sup>-1</sup>) [2, 3], are too low to satisfy the demands. Recently, lithium-sulfur (Li-S) battery has become increasingly attractive owing

to its high theoretical specific capacity (1,675 mAh·g<sup>-1</sup>) and energy density (2,567 Wh·kg<sup>-1</sup>) [4–6]. In addition, the cost can be significantly reduced because of the relative abundance of S in the Earth's crust. Nevertheless, the commercialization of Li-S batteries is limited by several obstacles [7]. First, both S and its solid reduction products (Li<sub>2</sub>S and Li<sub>2</sub>S<sub>2</sub>) are electrically insulating, so a significant portion of active materials cannot be utilized; thus, the overall specific capacity is reduced. Second, the volumetric expansion of S

Address correspondence to chongwuz@usc.edu

during cycling can be as large as 80% [8], which decreases the structural integrity of the entire cathode. Third, high-order polysulfides ( $S_x^{2-}$ ,  $3 \leq x \leq 8$ ) can be generated during the discharge/charge processes, and dissolve into the organic electrolyte. During cycling, these polysulfides shuttle to the surface of Li metal, and are reduced to insoluble  $Li_2S$  and  $Li_2S_2$ . This is the so-called shuttle effect, resulting in extremely poor cycling performance and low Coulombic efficiencies [9]. Then, if Li metal is used as the anode directly, Li dendrites that are formed during cycling can puncture the separator, leading to a short cycling life and severe safety issues [10].

In order to overcome the limitations mentioned above and realize Li-S batteries for practical applications, many strategies have been explored. For example, a conductive carbon matrix, which can work as the S host, has attracted extensive attention [8, 11–17]. Specifically, the free-standing conductive carbon nanofiber (CNF)/carbon nanotube (CNT) network, which has also been confirmed to be a promising candidate in other energy-storage devices [18–23], shows outstanding potential to overcome the insulating nature and volumetric expansion of S owing to its remarkable conductivity, large surface area, and good mechanical stability [24, 25]. Recently, a polysulfide-containing liquid catholyte has been reported to achieve a higher utilization of active materials because it avoids the insulating solid phase of S [26–28]. In addition, to further improve the performance, a number of studies focused on the suppression of the shuttle effect. For instance, a variety of porous carbon interlayers between the cathode and anode were used to absorb polysulfides during cycling [29–33]. However, the bare porous carbon interlayers did not solve the shuttle effect completely, and based on a previous report, the cycle life is still not long enough for practical applications [34, 35]. As a result, further research is still needed to improve the battery performance.

Besides highly porous carbon interlayers, certain gel polymers have previously been used as a gel electrolyte and can trap polysulfides [36–40]. In addition, the gel polymer can also provide a physical barrier to inhibit the internal shorting after long cycles and address the safety issues [41, 42]. In this

way, we believe that the family of gel polymers provides promising choices for interlayers; however, the Li-ion conductivity of most gel polymer electrolytes at room temperature is too low for directly utilization in Li-S batteries [42, 43]. Poly(vinylidene fluoride-co-hexafluoropropylene) (PVDF-HFP) is a copolymer that has been extensively studied as a gel polymer electrolyte [44–46], and it consists of crystalline poly(vinylidene difluoride) (PVDF), which can provide sufficient mechanical strength to form a free-standing film, and amorphous hexafluoropropylene (HFP), which can absorb large amounts of liquid electrolyte to improve the ionic conductivity. A phase-inversion technique [46, 47] was developed to form PVDF-HFP membranes with relatively high ionic conductivity ( $1.2 \times 10^{-3} S \cdot cm^{-1}$  at room temperature), making it an ideal candidate for polysulfide-trapping interlayers [36, 37, 48].

In the present work, our main goal is to create a PVDF-HFP+CNF composite interlayer, and to cap it onto a CNF+ $Li_2S_6$  composite cathode, thus forming a three-dimensional (3D) structural design (as illustrated in Fig. 1(a)) with a multitude of benefits. While CNF in the CNF+ $Li_2S_6$  cathode provides good electrical conduction and accommodates the volume expansion of the embedded sulfur, the PVDF-HFP layer can block the migration of polysulfides to suppress the shuttle effect, and our approach of embedding CNF into the PVDF-HFP layer can extend the electrical conduction to the polysulfides trapped in the PVDF-HFP, thus enabling the polysulfides to participate in the charging/discharging process [49]. Without PVDF-HFP in the interlayer, as shown in Fig. 1(b), dissolved polysulfides can migrate through the large pores of the CNF network, react with the Li anode, and form insoluble  $Li_2S/Li_2S_2$ , resulting in a rapid decrease in the capacity. However, when a pristine PVDF-HFP membrane without embedded CNFs is used as an interlayer, an increasing number of polysulfides will be absorbed over time, accumulate in the PVDF-HFP membrane, and lose electrical contact with the current collector, leading to a reduction in the total number of active materials (shown in Fig. 1(c)). Our 3D structural design results in a cathode showing impressive cycling performance at a current rate of 0.5 °C when the S

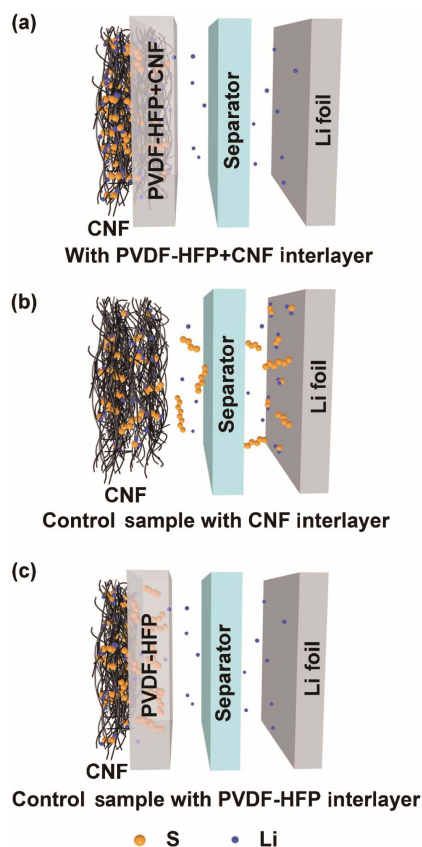


**Figure 1** Schematics of cells with (a) a PVDF-HFP+CNF interlayer, (b) a pristine CNF interlayer, and (c) a pristine PVDF-HFP interlayer after discharge processes. The brown particles, blue particles, and spaghetti-like black lines represent S, Li, and CNF, respectively. For clarity, the presence of PVDF-HFP can eliminate the shuttle effect of polysulfides, and the presence of CNF can recycle the S residues in the interlayer, leading to high specific capacities and good cyclability.

loading is  $1.7 \text{ mg}\cdot\text{cm}^{-2}$  (small capacity decay of 0.092% per cycle over 500 cycles). Furthermore, an excellent rate capability was also achieved up to  $2.0^\circ\text{C}$ . A detailed analysis demonstrates that the PVDF-HFP+CNF membrane plays an important role in the outstanding performance, while its excellent flexibility makes it a promising candidate for use in flexible batteries. The whole process is scalable and inexpensive, which is suitable for practical applications of Li-S batteries.

## 2 Experimental

### 2.1 Preparation of CNF free-standing networks

The method employed to prepare CNF free-standing networks is described below. The CNFs that we used

are commercially available PR-24-XT-HHT from Pyrograf Products, which was fully graphitized using a  $3,000^\circ\text{C}$  procedure for high conductivity, and has a specific surface area of  $34.9 \text{ m}^2\cdot\text{g}^{-1}$ , which was determined by performing Brunauer–Emmett–Teller (BET) analysis. The CNF free-standing networks were prepared using a convenient vacuum filtration method [20]. Before filtration, the CNFs were treated by a mixture of nitric acid ( $\text{HNO}_3$ ) and sulfuric acid ( $\text{H}_2\text{SO}_4$ ) to make them hydrophilic. The volumetric ratio of  $\text{HNO}_3$  and  $\text{H}_2\text{SO}_4$  was 3:1. In a typical acid treatment, 200-mg CNFs were well mixed with 20 mL acid solution and heated to  $90^\circ\text{C}$  for 10 h. The mixture was then diluted using 1 L deionized water, and was filtrated to obtain acid-treated CNFs. To prepare our desired CNF networks, 20 mg of acid-treated CNFs were well-dispersed in 20 mL of ethanol by ultra-sonication and stirring, followed by a vacuum filtration process. After drying, a CNF film can be peeled off from the filtration paper easily, and punched into  $1.5 \text{ cm}^2$  pieces. The total weight of a single CNF piece is about 2.8 mg.

### 2.2 Preparation of PVDF-HFP+CNF interlayers

The PVDF-HFP+CNF interlayers were prepared using a modified phase-inversion method [36, 46]. Commercially available PVDF-HFP was purchased from Sigma-Aldrich and dissolved in N-methyl pyrrolidone (NMP) solvent to prepare a 10% PVDF-HFP solution. The solution was placed in a  $60^\circ\text{C}$  oven for one week to ensure complete dissolution. Afterwards, acid-treated CNFs were mixed with the PVDF-HFP solution with a mass ratio of 1:40 (the mass ratio of CNF and pristine PVDF-HFP was 1:4) and milled into a slurry. The slurry was spread onto clean glass slides using a doctor blade, and then dried at  $60^\circ\text{C}$  in an oven for 1 h. After flowing water continuously, free-standing PVDF-HFP+CNF membranes can be peeled off easily and dried at  $60^\circ\text{C}$  overnight. Finally, the as-prepared PVDF-HFP+CNF membranes were punched into  $2 \text{ cm}^2$  pieces, which are slightly larger than the aforementioned CNF pieces. The total mass of the PVDF-HFP+CNF interlayer is about 3.1 mg.

### 2.3 Electrochemical measurements

An  $\text{Li}_2\text{S}_6$  solution with 4 molar sulfur in dimethoxyethane

(DME) was prepared using a solid-state stoichiometric reaction. Typically, 533-mg S powders and 154-mg  $\text{Li}_2\text{S}_6$  powders were mixed and added to 5-mL of DME. The mixture was stirred and heated up to 90 °C for two days to ensure a complete reaction. A specific amount of  $\text{Li}_2\text{S}_6$  solution was dropped onto CNF networks and dried to prepare an S cathode with various loadings. As the electrolyte, we used 1-M lithium bis(trifluoromethanesulfonyl)imide (LITFSI) in 1,2-DME and 1,3-dioxolane (DOL) (volume ratio 1:1) with 0.2 M of lithium nitrate ( $\text{LiNO}_3$ ) additive. A typical CR2032 coin cell was assembled using a piece of Li foil as the counter electrode with PVDF-HFP+CNF, pristine CNF, or pristine PVDF-HFP membrane as the interlayer between the S cathode and the separator. A total of 30  $\mu\text{L}$  of electrolyte was added on both sides of the interlayer. Cycling tests were carried out using a Neware battery testing instrument. The discharge/charge voltage range was 1.7–2.7 V, and 1 °C was defined as 1,675  $\text{mA}\cdot\text{g}^{-1}$ . The specific capacities were calculated based on the total mass of sulfur. The cyclic voltammetry (CV) and electrochemical impedance spectroscopy (EIS) measurements were performed on a Gamry electrochemical workstation.

## 2.4 Material characterization

The surface area of the CNF films was measured using a BET analyzer, and the sheet conductivity was measured using the four-probe method. The morphology of electrodes was characterized using a JEOL JSM-7001 scanning electron microscope (SEM) operated at 15 kV, which has analytical detectors for an energy-dispersive X-ray spectrometer (EDX). Samples after cycling were washed by DME twice to remove the electrolyte residue and dried in an argon-filled glovebox. To examine the absorption capability of PVDF-HFP, a 20- $\mu\text{L}$   $\text{Li}_2\text{S}_6$  solution was dropped onto both CNF and PVDF-HFP+CNF membranes. The as-prepared samples were dried in an Ar-filled glovebox and submerged into 2-mL DME for one day. A solution of 20- $\mu\text{L}$  pristine  $\text{Li}_2\text{S}_6$  was added to 2-mL DME as a control sample. The ultraviolet–visible (UV–vis) absorption spectra were collected using a Perkin-Elmer UV–vis–NIR spectrometer after diluting with a dilution factor of 2.

## 3 Results and discussion

Commercially available CNFs were treated using a strong acid and vacuum filtrated to form free-standing thin films. The BET surface area was measured as 34.9  $\text{m}^2\cdot\text{g}^{-1}$  (as shown in Fig. S1 in the Electronic Supplementary Material (ESM)). The sheet resistance of CNF films was determined to be 11  $\Omega\cdot\text{cm}^{-1}$  at 25 °C using the four-probe method, and the conductivity is calculated to be  $9.1 \times 10^2 \text{ S}\cdot\text{m}^{-1}$ . These porous and conductive CNF films were used as S reservoirs as well as current collectors. As can be seen from the SEM image shown in Fig. 2(a), the high porosity of the CNF network provides a large surface area for redox reactions, and a sufficient void space for the volume expansion. In addition, the interconnected CNFs enable fast electron transfer during cycling. Furthermore, the CNF network can also absorb and store liquid electrolytes with high ionic conductivity for fast Li-ion transfer during cycling. The cross-sectional SEM image of a pristine CNF S holder is shown in Fig. S2 (in the ESM), and its thickness is measured to be around 100  $\mu\text{m}$ . A specific amount of  $\text{Li}_2\text{S}_6$  was dissolved in the DME solvent and added to the CNF network by dropping and evaporation. The total amount of S in the CNF network can be controlled by the concentration of the  $\text{Li}_2\text{S}_6$  solution and the added volume. Typically, an  $\text{Li}_2\text{S}_6$  solution containing 4 molar sulfur was used owing to the proper viscosity for permeation. The SEM image of the as-prepared CNF+ $\text{Li}_2\text{S}_6$  cathode is shown in Fig. 2(b).  $\text{Li}_2\text{S}_6$  fills part of the void space and disperses uniformly across the CNF network. In general, the dimension of  $\text{Li}_2\text{S}_6$  is of the order of several micrometers, and almost no aggregated  $\text{Li}_2\text{S}_6$  was observed. The PVDF-HFP+CNF membrane was synthesized using a modified phase-inversion method, and the morphology is shown in Fig. 2(c). In a typical synthesis, 10% PVDF-HFP solution was prepared by dissolving a specific amount of commercial PVDF-HFP into the DME solvent. Then, acid-treated CNFs were ground in the PVDF-HFP solution (the mass ratio of PVDF-HFP and CNF was 4:1), and the slurry was spread onto clean glass slides, followed by drying at 60 °C for 1 h. Afterwards, the glass slides were rinsed with water, and free-standing PVDF-HFP+CNF membranes could be peeled off easily.



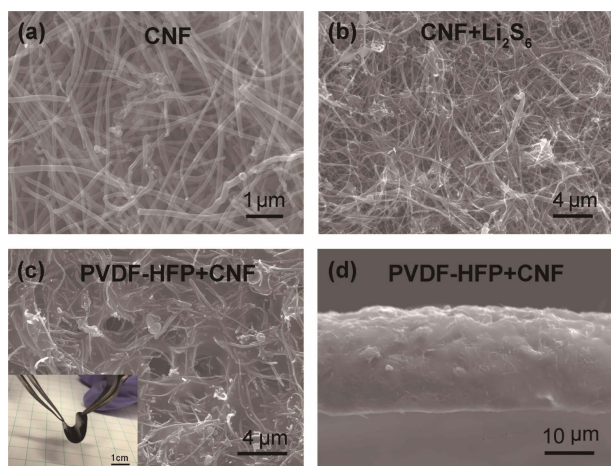


**Figure 2** Pre-cycle morphologies: SEM images of (a) the CNF S holder, (b) the CNF+Li<sub>2</sub>S<sub>6</sub> cathode, (c) the top view of the PVDF-HFP+CNF membrane (the inset is a photo to show the flexibility), and (d) a cross-sectional view of the PVDF-HFP+CNF membrane. The CNF S holder provides a large surface area, excellent conductivity, and sufficient mechanical strength to hold high loading of S, improve the electrical conductivity, and withstand the volume variation. However, the PVDF-HFP+CNF membrane works as a functional interlayer to avoid the shuttle effect and recycle the residue of S species.

Note that we rationally modified the traditional phase-inversion method. Traditionally, the non-solvent (water) is usually added to the PVDF-HFP solution before the solvent (NMP or acetone) was evaporated, resulting in highly porous membrane morphology [46, 47]. In our work, we first evaporated the NMP solvent at 60 °C for 1 h, and thus only a trace amount of NMP solvent existed in the hybrid membrane when exposed to water. In this way, the hybrid membrane can still be peeled off easily, and the membrane with less porosity can provide additional physical barriers to trap polysulfides. In contrast to a pristine CNF membrane, the hybrid gel membrane blocks the path for long-chain polysulfide migration; however, Li-ions can still move through the gel polymer electrolyte freely, and shuttle between the cathode and anode. Furthermore, the mechanical strength of the PVDF-HFP+CNF membrane was improved significantly compared with the pristine CNF membrane because the crystalline PVDF regions serve as physical cross-links. A photograph of the PVDF-HFP+CNF membrane is shown in the inset of Fig. 2(c), and it exhibits excellent flexibility, which is suitable even for flexible batteries. The cross-sectional SEM image of the PVDF-HFP+CNF membrane

is shown in Fig. 2(d). The thickness is only around 20 μm, which is sufficient to trap polysulfides, but would not contribute significantly to the total volume. After assembling a battery, the thickness of the CNF S holder was around 50 μm, and the thickness of the interlayer was around 6 μm inside the battery, as shown in Fig. S3 (in the ESM). The sheet resistance of the PVDF-HFP+CNF membrane was determined to be  $92 \Omega \cdot \square^{-1}$  at 25 °C using the four-probe method, and the electron conductivity is calculated to be  $5.6 \times 10^2 \text{ S} \cdot \text{m}^{-1}$ . The ion conductivity of the membrane was measured by EIS, and the test cell was assembled by sandwiching a piece of PVDF-HFP+CNF membrane between two stainless steel blocking electrodes [50]. The impedance spectrum is shown in Fig. S4 (in the ESM), and its ion conductivity is calculated to be  $2.1 \times 10^{-4} \text{ S} \cdot \text{cm}^{-1}$ .

In order to demonstrate the advantages of our proposed design, a series of electrochemical measurements were carried out. CNF+Li<sub>2</sub>S<sub>6</sub> films with various loading values of S were tested as the cathode, and Li metal foils were used as the anode. Additional pristine CNF membranes, pristine PVDF-HFP membranes, and the aforementioned PVDF-HFP+CNF membranes were used as interlayers for the control samples and experimental samples. To confirm the advantages of the PVDF-HFP+CNF membrane, the cyclability of the batteries was examined with different loading values of S at various current densities. The long-cycle stability of our proposed design with 1.7-mg·cm<sup>-2</sup> S is illustrated in Fig. 3(a). The cell with a PVDF-HFP+CNF interlayer exhibited stable discharge/charge capacities up to 500 cycles with a small degrading rate of 0.092% per cycle, which is much lower than the cell with a CNF interlayer (0.360% per cycle) and the cell with a PVDF-HFP interlayer (0.319% per cycle). Furthermore, the average Coulombic efficiency is calculated to be 98.3%, indicating high reversibility and excellent electrochemical stability. The rate capability of the experimental sample with 1.7-mg·cm<sup>-2</sup> S is shown in Fig. 3(b). The current rates were increased from 0.2 to 0.5, 1.0, 1.5, and 2.0 °C, and were finally kept at 1.0 °C. The battery with a PVDF-HFP+CNF interlayer exhibits high specific capacities and excellent capacity reversibility at all the discharge/charge rates. When the current rate was reset to 1.0 °C, there was no significant degradation up to

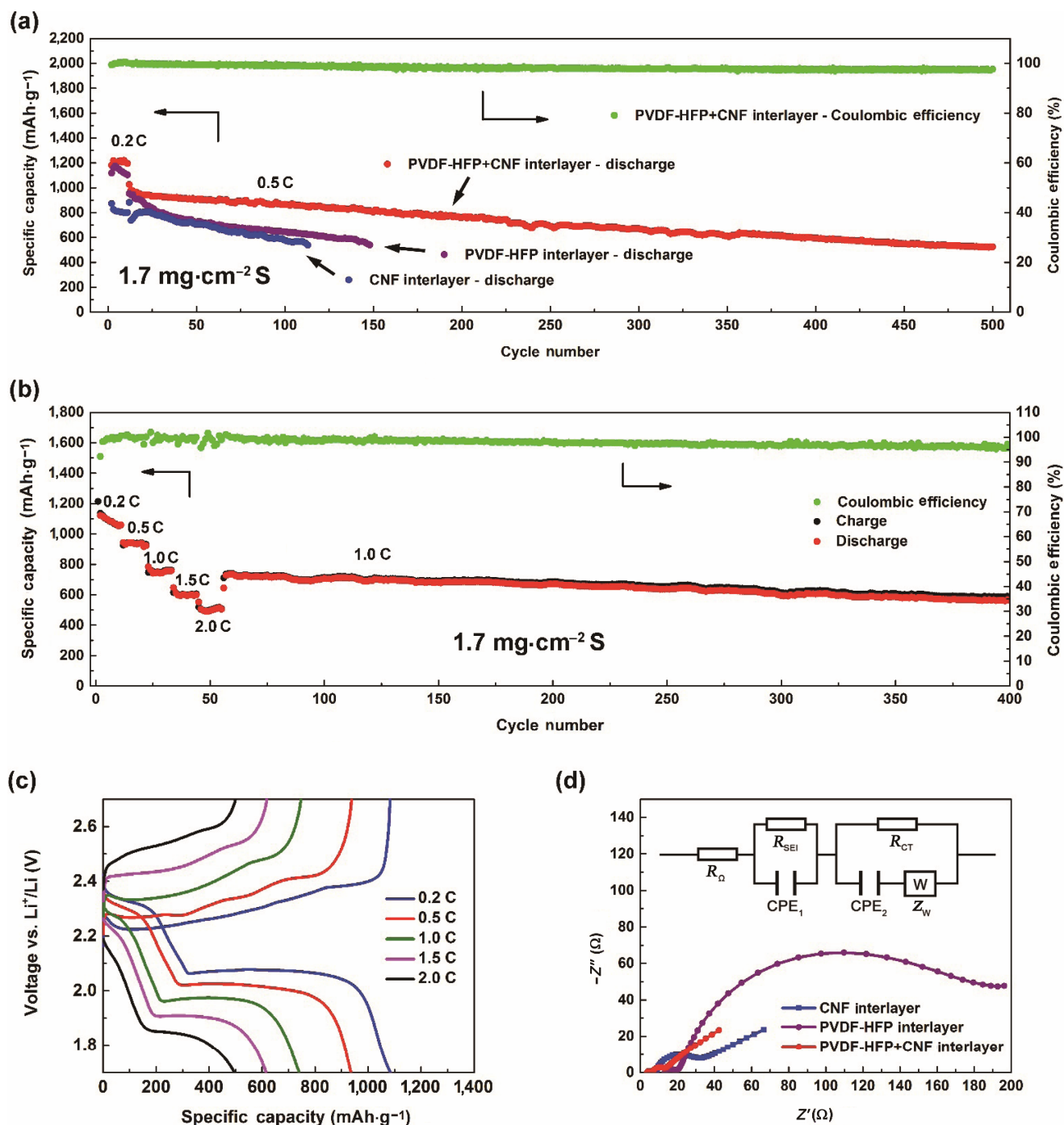


**Figure 3** Electrochemical characterizations: (a) long-cycle performance of batteries with a pristine CNF interlayer, a pristine PVDF-HFP interlayer and a PVDF-HFP+CNF interlayer when the loading is  $1.7 \text{ mg} \cdot \text{cm}^{-2} \text{ S}$ , and the current rate is  $0.5 \text{ C}$ , together with the Coulombic efficiencies of the battery with a PVDF-HFP+CNF interlayer; (b) rate capability of a battery with a PVDF-HFP+CNF interlayer when the S loading is  $1.7 \text{ mg} \cdot \text{cm}^{-2}$ ; (c) discharge/charge curves at various current densities for a battery with a PVDF-HFP+CNF interlayer; (d) Nyquist plots of batteries with a CNF interlayer, a PVDF-HFP interlayer, and a PVDF-HFP+CNF interlayer after the 10th discharge process, together with the corresponding equivalent circuit. All of the specific capacities were calculated based on the total mass of S.

400 cycles, and the degrading rate is only as small as 0.066% per cycle, suggesting that the whole structure

of our design remained intact after going through high current densities. In order to satisfy the demand

for practical applications, we increased the S loading to  $3.4 \text{ mg}\cdot\text{cm}^{-2}$  (as shown in Fig. S5 in the ESM). The cell with a PVDF-HFP+CNF interlayer still showed impressive retention of capacity over 300 cycles (small capacity decay of 0.125% per cycle). Figure S5 in the ESM shows the comparison of the cycling performance for three kinds of batteries: batteries with PVDF-HFP+CNF interlayer, batteries with only a CNF interlayer (i.e., no PVDF-HFP), and batteries with only a PVDF-HFP interlayer (i.e., no CNF). The data clearly show that batteries with a PVDF-HFP+CNF interlayer give the best performance. We compared the areal discharge specific capacities of our design after 100 cycles and 300 cycles with other recently published results that used the inexpensive CNF as the conductive matrix for Li-S, as shown in Table S1 in the ESM [17, 51–55]. Note that our 3D structural design enables outstanding performance in terms of both the areal specific capacity and cyclability. Figure 3(c) depicts the corresponding discharge/charge curves for the experimental samples at various current rates. The batteries were cycled between 1.7 and 2.7 V, and two flat voltage plateaus are observed at 0.2 °C during the discharge process. The higher discharge plateau around 2.3 V corresponds to the electrochemical transformation of solid sulfur ( $\text{S}_8$ ) to soluble long-chain polysulfides ( $\text{Li}_2\text{S}_x$ ,  $3 \leq x \leq 8$ ), and the lower discharge plateau close to 2.1 V is known to indicate the formation of insoluble  $\text{Li}_2\text{S}_2$  and  $\text{Li}_2\text{S}$ . Continuous charge plateaus from 2.2 to 2.4 V were also observed, and can be attributed to the successive conversion of  $\text{Li}_2\text{S}$  to  $\text{S}_8$ . When the current rates increased to 0.5, 1.0, 1.5, and 2.0 °C, obvious plateaus can still be observed within the same voltage window, confirming the excellent electrical conductivity of the cathode and good ionic conductivity of the gel interlayer. The CV profiles of batteries with PVDF-HFP+CNF collected at a scan rate of  $0.1 \text{ mV}\cdot\text{s}^{-1}$  are presented in Fig. S6 (in the ESM). Two separate reduction peaks and overlapped oxidation peaks were detected, which are typical in Li-S batteries, and are consistent with the discharge/charge plateaus. In addition, there was no significant difference between the CV curves of the 2nd cycle, the 5th cycle, the 10th cycle, and the 20th cycle, revealing the outstanding reversibility of batteries with a PVDF-HFP+CNF interlayer.

In order to further clarify the function of the PVDF-

HFP+CNF membrane, EIS was conducted after the 10th discharge process, as shown in Fig. 3(d). The Nyquist plots are composed of two depressed semicircles in the high-to-medium-frequency region and a straight line in the low-frequency region, which are typical for Li-S batteries, and which can be attributed to the solid-electrolyte interface (SEI) resistance ( $R_{\text{SEI}}$ ), the charge-transfer resistance ( $R_{\text{CT}}$ ), and the Warburg impedance. The intercept of the first semicircle at the  $Z'$  axis usually reflects the electrolyte resistance ( $R_{\Omega}$ ). After fitting the spectra with a suitable equivalent circuit model (the equivalent circuit is shown in the inset of Fig. 3(d), the fitted values are shown in Table S2 (in the ESM), and the fitting curves are shown in Fig. S7 in the ESM), the cell with a PVDF-HFP+CNF interlayer showed a much lower  $R_{\text{SEI}}$  and  $R_{\text{CT}}$  ( $R_{\text{SEI}} = 2.482 \Omega$ ,  $R_{\text{CT}} = 6.737 \Omega$ ) compared with the cell with a pristine CNF interlayer ( $R_{\text{SEI}} = 5.269 \Omega$ ,  $R_{\text{CT}} = 19.57 \Omega$ ). The reduction in the resistance after introducing PVDF-HFP indicates that this gel polymer electrolyte can limit the shuttling of polysulfides and effectively suppress the accumulation of electrically inert  $\text{Li}_2\text{S}/\text{Li}_2\text{S}_2$  on electrodes. The cell with a pristine PVDF-HFP membrane has a similar  $R_{\text{CT}}$  as the cell with a PVDF-HFP+CNF membrane; however, its  $R_{\Omega}$  (13.19) and  $R_{\text{SEI}}$  (143.0  $\Omega$ ) are much larger, indicating that the presence of CNF additives reduces the electrolyte resistance and shortens the ion-transfer distance effectively.

In order to understand the mechanism of the improvement from the PVDF-HFP+CNF membrane, post-cycle SEM images were taken. The cells with and without a PVDF-HFP+CNF interlayer were disassembled, and the PVDF-HFP+CNF interlayer and CNF S holders were washed by DME twice and dried in an Ar-filled glovebox before taking SEM images. Both sides of the PVDF-HFP+CNF interlayer were investigated after cycling for 20 cycles. The SEM image and the corresponding EDX spectrum of the side facing the Li metal anode are shown in Figs. 4(a) and 4(b), respectively. The surface of this side was very flat, and almost no deposited S species can be observed. Based on the EDX spectrum of this area, the atomic composition of S was as low as 0.22%. In comparison, the SEM image and the corresponding EDX spectrum of the side facing the CNF S holder are shown in Figs. 4(c) and 4(d), respectively. A large number of deposited S



species can be observed on the surface. The existence of a large amount of S can be further confirmed by the EDX spectrum in Fig. 4(d), and the atomic composition of S on this side was 6.29%, which was much larger than on the other side. The significant difference in the S composition on both sides confirms that the PVDF-HFP+CNF interlayer works as an effective physical barrier to hinder polysulfide migration, and only trace amounts of the S species can move through it [56]. Figure 4(e) shows an SEM image of a cathode from a cell without a PVDF-HFP+CNF interlayer after the 10th discharge process. A large number of solid residue accumulated on the surface of the CNFs, which was also reported in other conductive carbon matrices [57]. EDX was conducted, and the spectrum is shown in Fig. S8(a) (in the ESM). Only peaks for C, O, and S were present, which confirms the complete removal of electrolyte as no peak for F or N was observed. We believe that the residue was mainly composed of the insoluble and electrically insulating  $\text{Li}_2\text{S}/\text{Li}_2\text{S}_2$  or  $\text{S}_8$ , which does not participate in the charge/discharge processes, leading to a rapid degradation of the capacity. In addition, the undesired residue blocked the pores of the CNF network, hindered the Li-ion and electron transport, and resulted in high resistances, as shown by the EIS data. After longer cycles, an increasing amount of residue aggregated, and the pores would eventually be completely blocked, leading to the failure of the cell. In comparison, the SEM images of the CNF S holder from cells with PVDF-HFP+CNF after the 10th discharge process is shown in Fig. 4(f). Only micron-sized S species were deposited inside the CNF network (confirmed by the EDX spectrum in Fig. S8(b) in the ESM). Theoretically,  $\text{Li}_2\text{S}_x$  is reduced to  $\text{Li}_2\text{S}/\text{Li}_2\text{S}_2$  after discharging, and oxidized to elemental sulfur after charging, which is consistent with our observation. The small particles were trapped by the conductive CNF, and kept active during the discharge/charge processes. Similar morphology differences were also noticed after the 10th charge process, as shown in Fig. S9 (in the ESM), confirming the effectiveness of PVDF-HFP+CNF. Therefore, we believe that the PVDF-HFP gel polymer electrolyte suppressed the unreactive residue aggregation by covering the cathode surface closely, leading to a

high utilization rate of S species, and thus a long cycle life.

In order to further confirm the reversibility of the polysulfide trapping process in the interlayer, the cross-sectional morphologies of the 3D structures consisting of a PVDF-HFP+CNF interlayer and a CNF S holder after 10 cycles are shown in Fig. 5, together with the corresponding EDX mapping images of C, O, F, and S. The whole 3D structures were washed with DME three times to remove the electrolyte completely. In order to verify the successful removal of the electrolyte, a pristine PVDF-HFP+CNF membrane was soaked in the electrolyte and washed using the same method as a control experiment. The corresponding cross-sectional SEM and EDX mapping images are shown in Fig. S10 (in the ESM). Because there is almost no S signal in Fig. S10(e) (in the ESM), we can conclude that the electrolyte residue was removed completely with this method, and all the S signals in Fig. 5 came from the S species. Figures 5(a)–5(e) show the cross-sectional SEM and EDX mapping images at the interface of the CNF S holder and PVDF-HFP+CNF interlayer after the 10th discharge process. During the discharge process, a long-chain S species would be reduced to a short-chain S species and migrate towards the anode part. Based on the cross-sectional images and the corresponding EDX mapping images, more S species are dispersed in the PVDF-HFP+CNF interlayer than in the CNF S holder, indicating that the PVDF-HFP+CNF interlayer has a stronger trapping effect than the pristine CNF network. After the 10th charging process, the cross-sectional SEM and EDX mapping images at the interface are shown in Figs. 5(f)–5(j). It is clear that most of the S was dispersed in the CNF S holder, and almost no S signal can be detected in the PVDF-HFP+CNF interlayer. This demonstrates that the S species can move back to the CNF S holder during the charging process, and that the trapping process of the interlayer is highly reversible, which is confirmed by the excellent cyclic performance. In principle, much higher loadings of S can be achieved by stacking more layers of CNF S holders or PVDF-HFP+CNF interlayers, leading to a competitive areal energy density for practical applications.



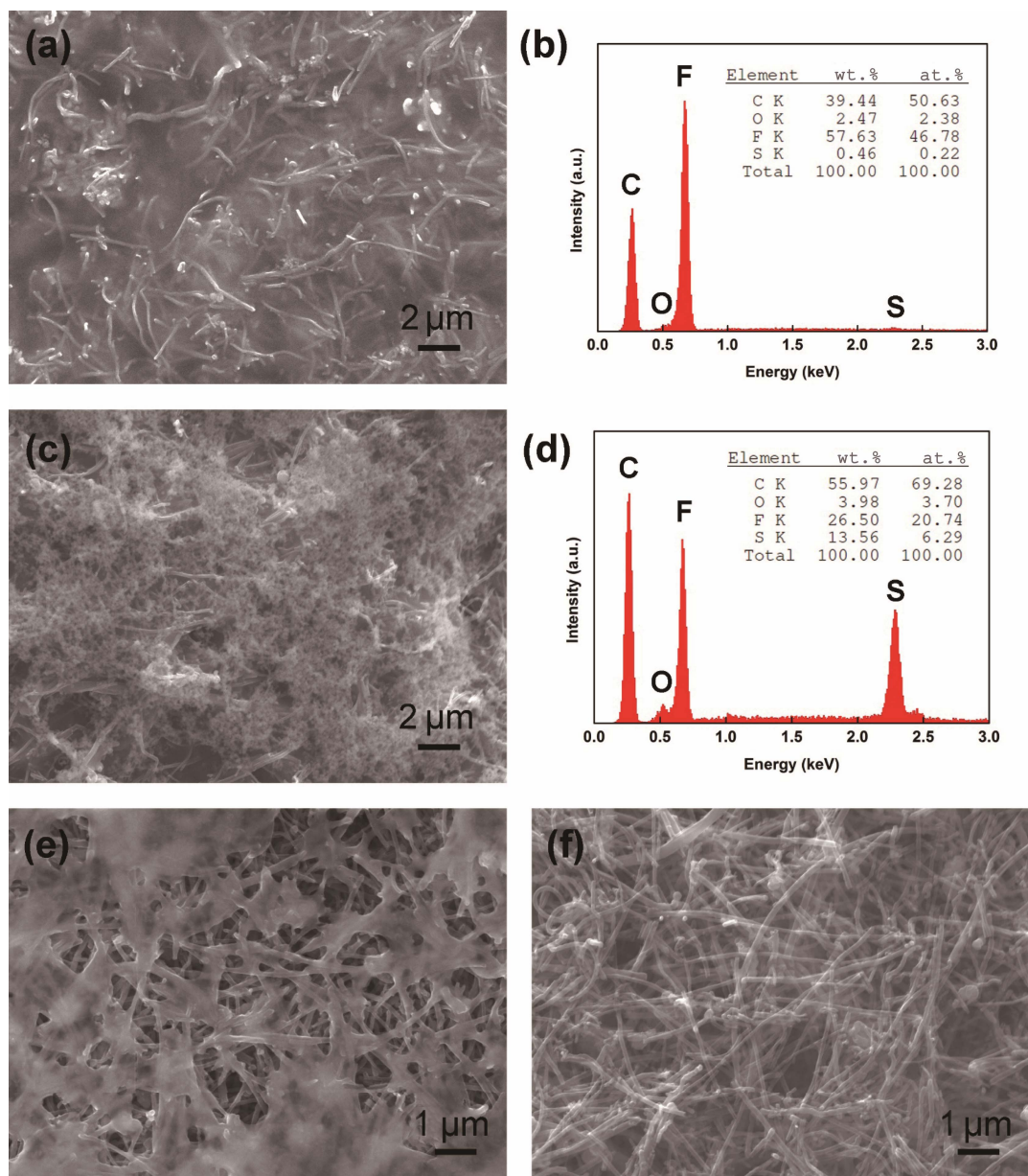


**Figure 4** Post-cycle surface morphology study: the SEM image (a) and EDX spectrum (b) of the side of the PVDF-HFP+CNF interlayer facing the Li metal anode (the inset of (b) shows the corresponding elemental composition) after 20 cycles; the SEM image (c) and EDX spectrum (d) of the side of the PVDF-HFP+CNF interlayer facing the CNF+Li<sub>2</sub>S<sub>6</sub> cathode (the inset of (d) shows the corresponding elemental composition) after 20 cycles; surface morphologies of CNF S holders from cells without (e) and with (f) a PVDF-HFP+CNF interlayer after the 10th discharge process. Here, the current density that we used was 0.2 °C. Compared with the side of the PVDF-HFP+CNF interlayer facing the CNF+Li<sub>2</sub>S<sub>6</sub> cathode, there is almost no sulfur deposition on the side facing the Li metal anode, demonstrating the effectiveness of the polysulfide trapping layer. Without PVDF-HFP, a large number of dead solid residue of S species accumulated on the surface of the CNF S holder and blocked the pores, resulting in a fast fading rate and short cycle life. However, with the protection by PVDF-HFP, only micron-sized particles were observed inside the CNF S holder, leading to a high utilization ratio and fast Li-ion/electron transport.

To verify the polysulfide-trapping capability of the PVDF-HFP+CNF interlayer, we performed an absorption test, as described below. 20  $\mu$ L of 4-M Li<sub>2</sub>S<sub>6</sub> solution (based on the S mass) was placed onto both CNF

and PVDF-HFP+CNF interlayers. The two pieces of interlayers were dried in an Ar-filled glovebox and immersed in 2-mL DME solvent separately. After soaking for one day, a significant color difference was

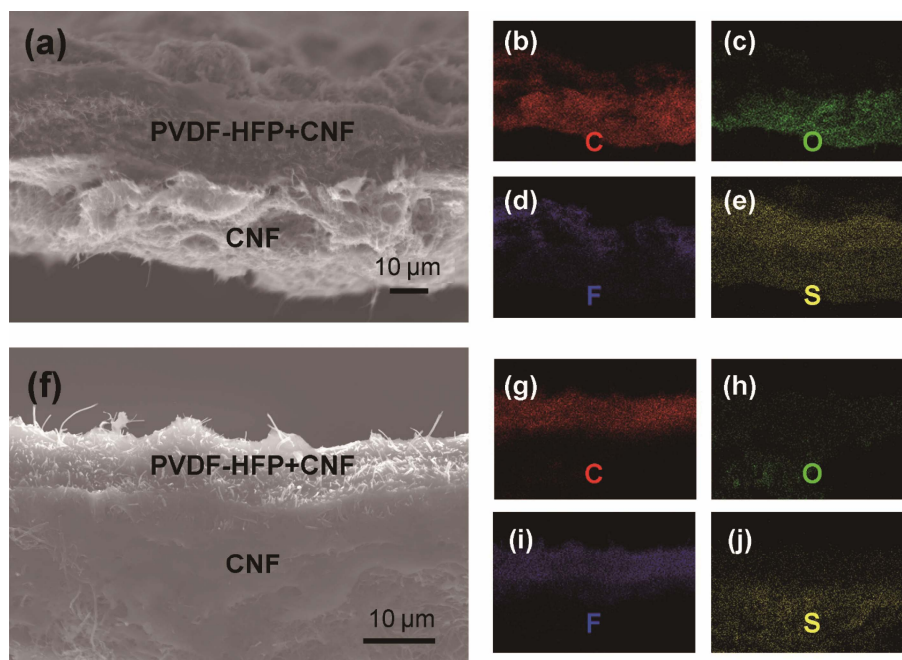


**Figure 5** Post-cycle cross-sectional SEM images and EDX mappings at the interface of the CNF S holder and PVDF-HFP+CNF interlayer: (a) cross-sectional morphologies after the 10th discharging process; EDX mapping of (b) C, (c) O, (d) F, and (e) S for the area in (a); (f) cross-sectional morphologies after the 10th charging process; EDX mapping of (g) C, (h) O, (i) F, and (j) S for the area in (f). Based on the cross-sectional and EDX mapping images, S species were trapped by the PVDF-HFP+CNF interlayer after the discharging process, and returned to the CNF S holder after the charging process, indicating the reversibility of the polysulfide trapping process.

observed, as shown in Fig. S11(a) (in the ESM). The sample with the CNF interlayer became dark brown, which is similar to the pristine  $\text{Li}_2\text{S}_6$  solution. However, the sample with the PVDF-HFP+CNF interlayer is relatively transparent with a slight yellow color, indicating that most of the  $\text{Li}_2\text{S}_6$  was still preserved in the PVDF-HFP copolymer. To analyze the S concentration quantitatively, a series of UV-vis spectra were taken from the diluted samples, as shown in Fig. S11(b) (in the ESM). Compared with  $\text{CNF}+\text{Li}_2\text{S}_6$ , a weaker band close to 300 nm, which corresponds to  $\text{S}_6^{2-}$  [58], was shown in the  $\text{PVDF-HFP}+\text{CNF}+\text{Li}_2\text{S}_6$  sample. This indicates that less  $\text{Li}_2\text{S}_6$  was present in the solution, and thus more  $\text{Li}_2\text{S}_6$  remained in PVDF-HFP. This strongly supports our analysis that PVDF-HFP can suppress the migration of polysulfides to the anode, thus alleviating the shuttle effect.

## 4 Conclusions

In summary, we developed a feasible and low-cost 3D structure for Li-S batteries by capping a flexible PVDF-HFP+CNF gel membrane onto a free-standing

and binder-free  $\text{CNF}+\text{Li}_2\text{S}_6$  composite cathode. While the CNF network provides excellent conductivity for electron transport, a large surface area to hold active materials, and strong mechanical stability to endure volume expansion, the functional PVDF-HFP+CNF interlayer is permeable to Li-ions, while it hinders the shuttling of polysulfides and extends the electrical conduction of the CNF current collector to help with the recycling of active materials. As a result, high and reversible capacities up to 500 cycles were achieved with an S loading of  $1.7 \text{ mg}\cdot\text{cm}^{-2}$  (a small capacity decay of 0.092% per cycle). In addition, the proposed 3D structure enables stable cycling at even higher current rates (1.0 to 2.0 °C). The whole production process is inexpensive, scalable, and environmentally friendly, making it a practical candidate for various commercial applications.

## Acknowledgements

The SEM images used in this article were generated at the Center for Electron Microscopy and Microanalysis, University of Southern California. The EIS data used

in this article was collected in Dr. Stephen Cronin's lab. The BET data used in this article was collected in Dr. Richard L. Brutchey's lab.

**Electronic Supplementary Material:** Supplementary material (comparison with other recent reports, nitrogen sorption isotherm, supporting SEM and EDX data, supporting impedance spectra, the cycling stability with higher S loading, CV curves and the results of absorption test) is available in the online version of this article at <https://doi.org/10.1-007/s12274-017-1929-0>.

## References

- [1] Mizushima, K.; Jones, P. C.; Wiseman, P. J.; Goodenough, J. B.  $\text{Li}_x\text{CoO}_2$  ( $0 < x \leq 1$ ): A new cathode material for batteries of high energy density. *Mat. Res. Bull.* **1980**, *15*, 783–789.
- [2] Padhi, A. K.; Nanjundaswamy, K. S.; Goodenough, J. B. Phospho-olivines as positive-electrode materials for rechargeable lithium batteries. *J. Electrochem. Soc.* **1997**, *144*, 1188–1194.
- [3] Nitta, N.; Wu, F. X.; Lee, J. T.; Yushin, G. Li-ion battery materials: Present and future. *Mater. Today* **2015**, *18*, 252–264.
- [4] Ji, X. L.; Lee, K. T.; Nazar, L. F. A highly ordered nanostructured carbon-sulphur cathode for lithium-sulphur batteries. *Nat. Mater.* **2009**, *8*, 500–506.
- [5] Wang, H. L.; Yang, Y.; Liang, Y. Y.; Robinson, J. T.; Li, Y. G.; Jackson, A.; Cui, Y.; Dai, H. J. Graphene-wrapped sulfur particles as a rechargeable lithium-sulfur battery cathode material with high capacity and cycling stability. *Nano Lett.* **2011**, *11*, 2644–2647.
- [6] Jayaprakash, N.; Shen, J.; Moganty, S. S.; Corona, A.; Archer, L. A. Porous hollow carbon@sulfur composites for high-power lithium-sulfur batteries. *Angew. Chem., Int. Ed.* **2011**, *50*, 5904–5908.
- [7] Manthiram, A.; Fu, Y. Z.; Su, Y.-S. Challenges and prospects of lithium-sulfur batteries. *Acc. Chem. Res.* **2013**, *46*, 1125–1134.
- [8] Fang, R. P.; Zhao, S. Y.; Pei, S. F.; Qian, X. T.; Hou, P. X.; Cheng, H. M.; Liu, C.; Li, F. Toward more reliable lithium-sulfur batteries: An all-graphene cathode structure. *ACS Nano* **2016**, *10*, 8676–8682.
- [9] Busche, M. R.; Adelhelm, P.; Sommer, H.; Schneider, H.; Leitner, K.; Janek, J. Systematical electrochemical study on the parasitic shuttle-effect in lithium-sulfur-cells at different temperatures and different rates. *J. Power Sources* **2014**, *259*, 289299.
- [10] Crowther, O.; West, A. C. Effect of electrolyte composition on lithium dendrite growth. *J. Electrochem. Soc.* **2008**, *155*, A806–A811.
- [11] Zhou, G. M.; Paek, E.; Hwang, G. S.; Manthiram, A. Long-life Li/polysulphide batteries with high sulphur loading enabled by lightweight three-dimensional nitrogen/sulphur-codoped graphene sponge. *Nat. Commun.* **2015**, *6*, 7760.
- [12] Li, G. X.; Sun, J. H.; Hou, W. P.; Jiang, S. D.; Huang, Y.; Geng, J. X. Three-dimensional porous carbon composites containing high sulfur nanoparticle content for high-performance lithium-sulfur batteries. *Nat. Commun.* **2016**, *7*, 10601.
- [13] Cheng, X.-B.; Huang, J.-Q.; Zhang, Q.; Peng, H.-J.; Zhao, M.-Q.; Wei, F. Aligned carbon nanotube/sulfur composite cathodes with high sulfur content for lithium-sulfur batteries. *Nano Energy* **2014**, *4*, 65–72.
- [14] Huang, J.-Q.; Liu, X.-F.; Zhang, Q.; Chen, C.-M.; Zhao, M.-Q.; Zhang, S.-M.; Zhu, W.; Qian, W.-Z.; Wei, F. Entrapment of sulfur in hierarchical porous graphene for lithium-sulfur batteries with high rate performance from  $-40$  to  $60^\circ\text{C}$ . *Nano Energy* **2013**, *2*, 314–321.
- [15] Zhao, M. Q.; Zhang, Q.; Huang, J. Q.; Tian, G. L.; Nie, J. Q.; Peng, H. J.; Wei, F. Unstacked double-layer templated graphene for high-rate lithium-sulphur batteries. *Nat. Commun.* **2014**, *5*, 3410.
- [16] Zhao, M. Q.; Liu, X. F.; Zhang, Q.; Tian, G. L.; Huang, J. Q.; Zhu, W. C.; Wei, F. Graphene/single-walled carbon nanotube hybrids: One-step catalytic growth and applications for high-rate Li-S batteries. *ACS Nano* **2012**, *6*, 10759–10769.
- [17] Zheng, G. Y.; Yang, Y.; Cha, J. J.; Hong, S. S.; Cui, Y. Hollow carbon nanofiber-encapsulated sulfur cathodes for high specific capacity rechargeable lithium batteries. *Nano Lett.* **2011**, *11*, 4462–4467.
- [18] Fang, X.; Shen, C. F.; Ge, M. Y.; Rong, J. P.; Liu, Y. H.; Zhang, A. Y.; Wei, F.; Zhou, C. W. High-power lithium ion batteries based on flexible and light-weight cathode of  $\text{LiNi}_{0.5}\text{Mn}_{1.5}\text{O}_4$ /carbon nanotube film. *Nano Energy* **2015**, *12*, 43–51.
- [19] Liu, Y. H.; Fang, X.; Ge, M. Y.; Rong, J. P.; Shen, C. F.; Zhang, A. Y.; Enaya, H. A.; Zhou, C. W.  $\text{SnO}_2$  coated carbon cloth with surface modification as Na-ion battery anode. *Nano Energy* **2015**, *16*, 399–407.
- [20] Zhang, A. Y.; Fang, X.; Shen, C. F.; Liu, Y. H.; Zhou, C. W. A carbon nanofiber network for stable lithium metal anodes with high Coulombic efficiency and long cycle life. *Nano Res.* **2016**, *9*, 3428–3436.
- [21] Xu, Z.-L.; Zhang, B.; Kim, J.-K. Electrospun carbon nanofiber anodes containing monodispersed Si nanoparticles and graphene oxide with exceptional high rate capacities. *Nano Energy* **2014**, *6*, 27–35.
- [22] Cheng, Y. L.; Huang, L.; Xiao, X.; Yao, B.; Yuan, L. Y.; Li, T. Q.; Hu, Z. M.; Wang, B.; Wan, J.; Zhou, J. Flexible and cross-linked N-doped carbon nanofiber network for high performance freestanding supercapacitor electrode. *Nano Energy* **2015**, *15*, 66–74.
- [23] Li, M. Y.; Zu, M.; Yu, J. S.; Cheng, H. F.; Li, Q. W. Stretchable

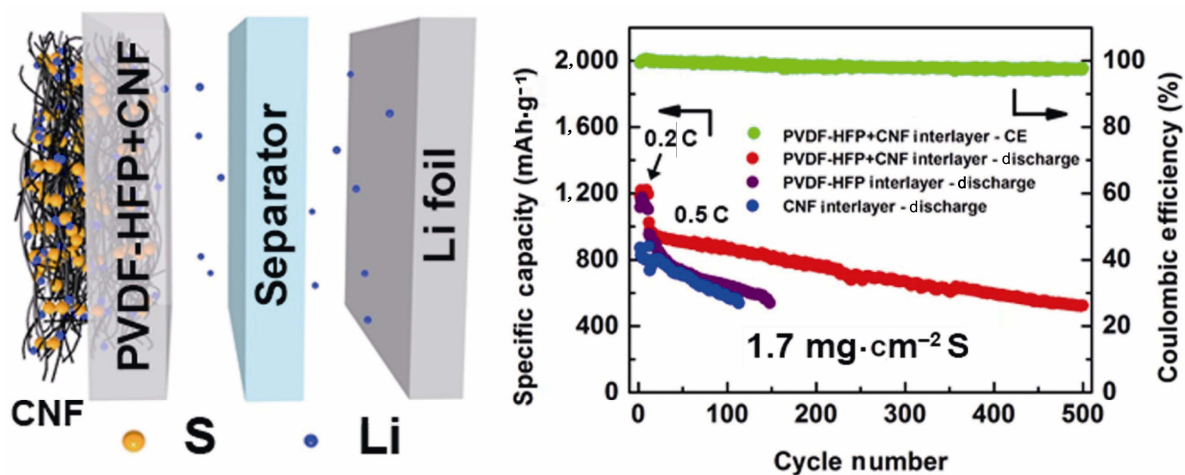


- fiber supercapacitors with high volumetric performance based on buckled MnO<sub>2</sub>/oxidized carbon nanotube fiber electrodes. *Small* **2017**, *13*, 1602994.
- [24] Elazari, R.; Salitra, G.; Garsuch, A.; Panchenko, A.; Aurbach, D. Sulfur-impregnated activated carbon fiber cloth as a binder-free cathode for rechargeable Li-S batteries. *Adv. Mater.* **2011**, *23*, 5641–5644.
- [25] Zhou, G. M.; Wang, D. W.; Li, F.; Hou, P. X.; Yin, L. C.; Liu, C.; Lu, G. Q.; Gentle, I. R.; Cheng, H.-M. A flexible nanostructured sulphur–carbon nanotube cathode with high rate performance for Li-S batteries. *Energy Environ. Sci.* **2012**, *5*, 8901–8906.
- [26] Yao, H.; Zheng, G.; Hsu, P. C.; Kong, D.; Cha, J. J.; Li, W.; Seh, Z. W.; McDowell, M. T.; Yan, K.; Liang, Z. et al. Improving lithium-sulphur batteries through spatial control of sulphur species deposition on a hybrid electrode surface. *Nat. Commun.* **2014**, *5*, 3943.
- [27] Yu, X. W.; Manthiram, A. A class of polysulfide catholytes for lithium-sulfur batteries: Energy density, cyclability, and voltage enhancement. *Phys. Chem. Chem. Phys.* **2015**, *17*, 2127–2136.
- [28] Pu, X.; Yang, G.; Yu, C. Liquid-type cathode enabled by 3D sponge-like carbon nanotubes for high energy density and long cycling life of Li-S batteries. *Adv. Mater.* **2014**, *26*, 7456–7461.
- [29] Xiao, Z. B.; Yang, Z.; Wang, L.; Nie, H. G.; Zhong, M. E.; Lai, Q. Q.; Xu, X. J.; Zhang, L. J.; Huang, S. M. A lightweight TiO<sub>2</sub>/graphene interlayer, applied as a highly effective polysulfide absorbent for fast, long-life lithium-sulfur batteries. *Adv. Mater.* **2015**, *27*, 2891–2898.
- [30] Su, Y. S.; Manthiram, A. Lithium-sulphur batteries with a microporous carbon paper as a bifunctional interlayer. *Nat. Commun.* **2012**, *3*, 1166.
- [31] Su, Y. S.; Manthiram, A. A new approach to improve cycle performance of rechargeable lithium-sulfur batteries by inserting a free-standing MWCNT interlayer. *Chem. Commun.* **2012**, *48*, 8817–8819.
- [32] Zhou, G. M.; Pei, S. F.; Li, L.; Wang, D. W.; Wang, S. G.; Huang, K.; Yin, L. C.; Li, F.; Cheng, H. M. A graphene-pure-sulfur sandwich structure for ultrafast, long-life lithium-sulfur batteries. *Adv. Mater.* **2014**, *26*, 625–631.
- [33] Liu, M.; Qin, X. Y.; He, Y. B.; Li, B. H.; Kang, F. Y. Recent innovative configurations in high-energy lithium-sulfur batteries. *J. Mater. Chem. A* **2017**, *5*, 5222.
- [34] Kim, H. M.; Hwang, J. Y.; Manthiram, A.; Sun, Y. K. High-performance lithium-sulfur batteries with a self-assembled multiwall carbon nanotube interlayer and a robust electrode-electrolyte interface. *ACS Appl. Mater. Interfaces* **2016**, *8*, 983–987.
- [35] Ma, Z. L.; Li, Z.; Hu, K.; Liu, D. D.; Huo, J.; Wang, S. Y. The enhancement of polysulfide absorption in LiS batteries by hierarchically porous CoS<sub>2</sub>/carbon paper interlayer. *J. Power Sources* **2016**, *325*, 71–78.
- [36] Shin, J. H.; Jung, S. S.; Kim, K. W.; Ahn, H. J. Preparation and characterization of plasticized polymer electrolytes based on the PVdF-HFP copolymer for lithium/sulfur battery. *J. Mater. Sci. Mater. Electron.* **2002**, *13*, 727–733.
- [37] Wang, J.; Yang, J.; Wan, C.; Du, K.; Xie, J.; Xu, N. Sulfur composite cathode materials for rechargeable lithium batteries. *Adv. Funct. Mater.* **2003**, *13*, 487–492.
- [38] Zhang, S. S.; Tran, D. T. How a gel polymer electrolyte affects performance of lithium/sulfur batteries. *Electrochim. Acta* **2013**, *114*, 296–302.
- [39] Rao, M. M.; Geng, X. Y.; Li, X. P.; Hu, S. J.; Li, W. S. Lithium-sulfur cell with combining carbon nanofibers–sulfur cathode and gel polymer electrolyte. *J. Power Sources* **2012**, *212*, 179–185.
- [40] Liu, M.; Ren, Y. X.; Zhou, D.; Jiang, H. R.; Kang, F. Y.; Zhao, T. S. A lithium/polysulfide battery with dual-working mode enabled by liquid fuel and acrylate-based gel polymer electrolyte. *ACS Appl. Mater. Interfaces* **2017**, *9*, 2526–2534.
- [41] Tatsuma, T.; Taguchi, M.; Oyama, N. Inhibition effect of covalently cross-linked gel electrolytes on lithium dendrite formation. *Electrochim. Acta* **2001**, *46*, 1201–1205.
- [42] Manuel Stephan, A. Review on gel polymer electrolytes for lithium batteries. *Eur. Polym. J.* **2006**, *42*, 21–42.
- [43] Zhao, Y.; Zhang, Y. G.; Gosselink, D.; Doan, T. N.; Sadhu, M.; Cheang, H. J.; Chen, P. Polymer electrolytes for lithium/sulfur batteries. *Membranes* **2012**, *2*, 553–564.
- [44] Stephan, A. M.; Saito, Y. Ionic conductivity and diffusion coefficient studies of PVdF-HFP polymer electrolytes prepared using phase inversion technique. *Solid State Ion.* **2002**, *148*, 475–481.
- [45] Cao, J. H.; Zhu, B. K.; Xu, Y. Y. Structure and ionic conductivity of porous polymer electrolytes based on PVDF-HFP copolymer membranes. *J. Membrane Sci.* **2006**, *281*, 446–453.
- [46] Kim, K. M.; Park, N. G.; Ryu, K. S.; Chang, S. H. Characteristics of PVdF-HFP/TiO<sub>2</sub> composite membrane electrolytes prepared by phase inversion and conventional casting methods. *Electrochim. Acta* **2006**, *51*, 5636–5644.
- [47] Pu, W. H.; He, X. M.; Wang, L.; Jiang, C. Y.; Wan, C. R. Preparation of PVDF-HFP microporous membrane for Li-ion batteries by phase inversion. *J. Membrane Sci.* **2006**, *272*, 11–14.
- [48] Wang, J. L.; Yang, J.; Xie, J. Y.; Xu, N. X.; Li, Y. Sulfur-carbon nano-composite as cathode for rechargeable lithium battery based on gel electrolyte. *Electrochem. Commun.* **2002**, *4*, 499–502.
- [49] Yao, H. B.; Yan, K.; Li, W. Y.; Zheng, G. Y.; Kong, D. S.; Seh, Z. W.; Narasimhan, V. K.; Liang, Z.; Cui, Y. Improved lithium-sulfur batteries with a conductive coating on the separator to prevent the accumulation of inactive S-related species at the cathode-separator interface. *Energy Environ. Sci.* **2014**, *7*,



- 3381–3390.
- [50] Abraham, K. M.; Jiang, Z.; Carroll, B. Highly conductive PEO-like polymer electrolytes. *Chem. Mater.* **1997**, *9*, 1978–1988.
- [51] Yang, J.; Xie, J.; Zhou, X. Y.; Zou, Y. L.; Tang, J. J.; Wang, S. C.; Chen, F.; Wang, L. Y. Functionalized N-doped porous carbon nanofiber webs for a lithium–sulfur battery with high capacity and rate performance. *J. Phys. Chem. C* **2014**, *118*, 1800–1807.
- [52] Li, Q.; Zhang, Z. A.; Zhang, K.; Fang, J.; Lai, Y. Q.; Li, J. A simple synthesis of hollow carbon nanofiber-sulfur composite via mixed-solvent process for lithium–sulfur batteries. *J. Power Sources* **2014**, *256*, 137–144.
- [53] Zheng, G. Y.; Zhang, Q. F.; Cha, J. J.; Yang, Y.; Li, W. Y.; Seh, Z. W.; Cui, Y. Amphiphilic surface modification of hollow carbon nanofibers for improved cycle life of lithium sulfur batteries. *Nano Lett.* **2013**, *13*, 1265–1270.
- [54] Yao, H. B.; Zheng, G. Y.; Li, W. Y.; McDowell, M. T.; Seh, Z. W.; Liu, N.; Lu, Z. D.; Cui, Y. Crab shells as sustainable templates from nature for nanostructured battery electrodes. *Nano Lett.* **2013**, *13*, 3385–3390.
- [55] Lu, S. T.; Cheng, Y. W.; Wu, X. H.; Liu, J. Significantly improved long-cycle stability in high-rate Li-S batteries enabled by coaxial graphene wrapping over sulfur-coated carbon nanofibers. *Nano Lett.* **2013**, *13*, 2485–2489.
- [56] Jeddi, K.; Sarikhani, K.; Qazvini, N. T.; Chen, P. Stabilizing lithium/sulfur batteries by a composite polymer electrolyte containing mesoporous silica particles. *J. Power Sources* **2014**, *245*, 656–662.
- [57] Yoo, J.; Cho, S. J.; Jung, G. Y.; Kim, S. H.; Choi, K. H.; Kim, J. H.; Lee, C. K.; Kwak, S. K.; Lee, S. Y. COF-net on CNT-net as a molecularly designed, hierarchical porous chemical trap for polysulfides in lithium-sulfur batteries. *Nano Lett.* **2016**, *16*, 3292–3300.
- [58] Barchasz, C.; Molton, F.; Duboc, C.; Lepretre, J. C.; Patoux, S.; Alloin, F. Lithium/sulfur cell discharge mechanism: An original approach for intermediate species identification. *Anal. Chem.* **2012**, *84*, 3973–3980.

## Table of contents



In order to address the challenges associated with the use of lithium-sulfur (Li-S) batteries, we created a poly(vinylidene fluoride-co-hexafluoropropylene) (PVDF-HFP)+carbon nanofiber (CNF) composite interlayer and capped it onto a CNF+Li<sub>2</sub>S<sub>6</sub> composite cathode, thus forming a three-dimensional (3D) structural design with multitude advantages, thus enabling outstanding long-cycling performance.

## Electronic Supplementary Material

# Functional interlayer of PVDF-HFP and carbon nanofiber for long-life lithium-sulfur batteries

Anyi Zhang<sup>1,§</sup>, Xin Fang<sup>1,§</sup>, Chenfei Shen<sup>1</sup>, Yihang Liu<sup>2</sup>, In Gi Seo<sup>1</sup>, Yuqiang Ma<sup>3</sup>, Liang Chen<sup>2</sup>, Patrick Cottingham<sup>4</sup>, and Chongwu Zhou<sup>2</sup> (✉)

<sup>1</sup> Mork Family Department of Chemical Engineering and Materials Science, University of Southern California, Los Angeles, California 90089, USA

<sup>2</sup> Ming Hsieh Department of Electrical Engineering, University of Southern California, Los Angeles, California 90089, USA

<sup>3</sup> Department of Physics and Astronomy, University of Southern California, Los Angeles, California 90089, USA

<sup>4</sup> Department of Chemistry, University of Southern California, Los Angeles, California 90089, USA

<sup>§</sup> Anyi Zhang and Xin Fang contributed equally in this work

Supporting information to <https://doi.org/10.1007/s12274-017-1929-0>

**Table S1** Detailed comparison of this work with other Li-S battery works that utilized the inexpensive carbon nanofiber as conductive matrix. [1-6]

Work	S Loading (mg/cm <sup>2</sup> )	Rate (C)	Discharge Capacity after 100 cycles (mAh/g)	Areal Capacity after 100 cycles (mAh/cm <sup>2</sup> )	Discharge Capacity after 300 cycles (mAh/g)	Areal Capacity after 300 cycles (mAh/cm <sup>2</sup> )
This Work	1.7	0.5	868	1.48	671	1.14
		1	729	1.24	595	1.01
	3.4	0.5	647	2.29	524	1.78
Ref.1	1	0.5	700	0.7	—	—
Ref.2	0.95	0.5	820	0.779	—	—
		1	700	0.665	—	—
Ref.3	1.5	1	600	0.9	—	—
Ref.4	1.5	0.5	790	1.185	620	0.93
Ref.5	0.8	0.5	700	0.56	—	—
Ref.6	0.99	1	370	0.366	340	0.337

**Table S2** Comparison of  $R_{\Omega}$ ,  $R_{SEI}$  and  $R_{CT}$  for batteries with CNF, PVDF-HFP and PVDF-HFP+CNF interlayers after the 10th discharge process.  $R_{\Omega}$ ,  $R_{SEI}$ , and  $R_{CT}$  represents the electrolyte resistance, the SEI resistance and the charge-transfer resistance, respectively.

	$R_{\Omega}$ ( $\Omega$ )	$R_{SEI}$ ( $\Omega$ )	$R_{CT}$ ( $\Omega$ )
With CNF	4.751	5.269	19.57
With PVDF-HFP	13.19	143.0	6.537
With PVDF-HFP+CNF	3.686	2.482	6.737

Address correspondence to [chongwuz@usc.edu](mailto:chongwuz@usc.edu)

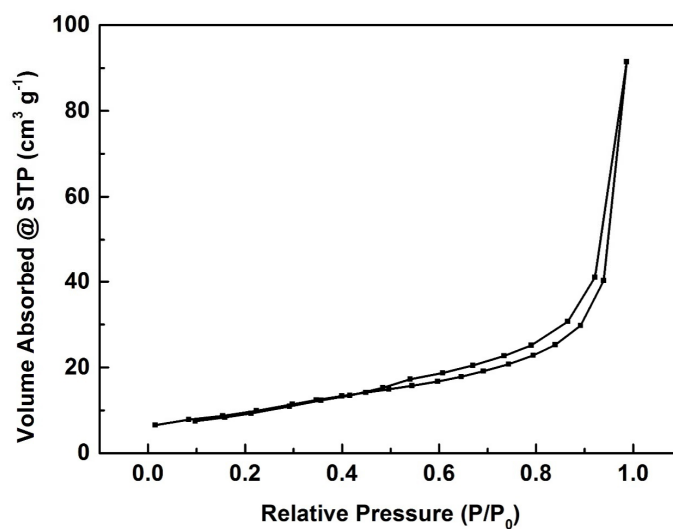


**Figure S1** Nitrogen sorption isotherm of CNF.

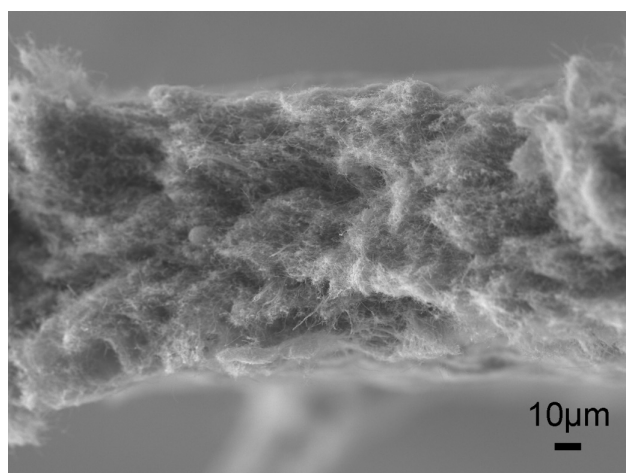


**Figure S2** The cross-sectional SEM image of a pristine CNF film

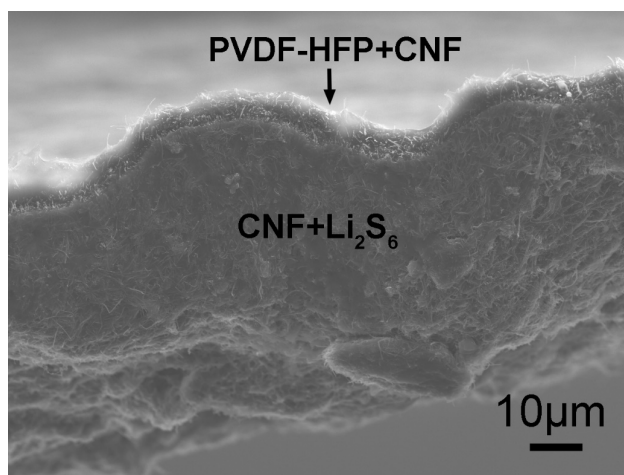


**Figure S3** The cross-sectional SEM image of a CNF+Li<sub>2</sub>S<sub>6</sub> cathode capped by a PVDF-HFP+CNF interlayer from a disassembled coin cell.



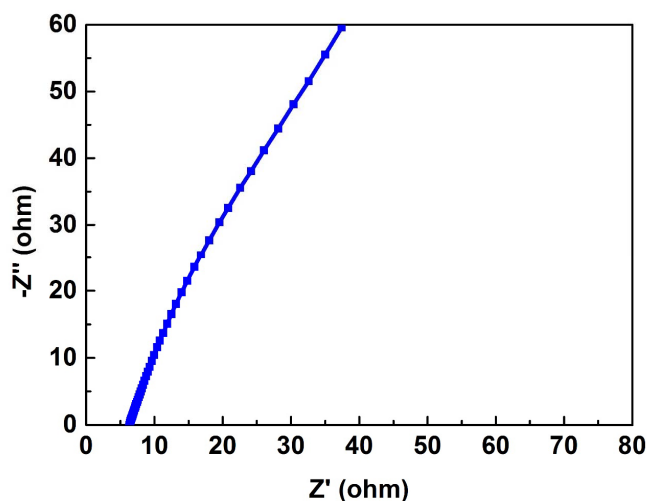


**Figure S4** Impedance spectrum of a PVDF-HFP+CNF membrane at 25 °C, recorded between stainless steel blocking electrodes.

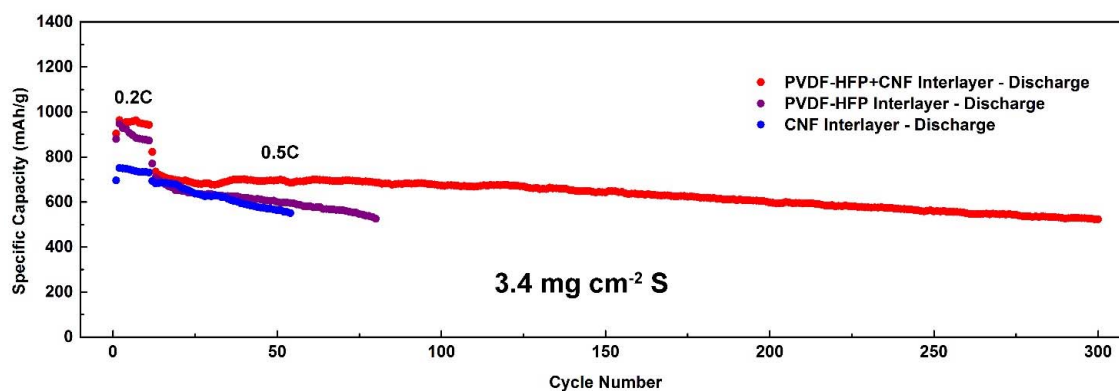


**Figure S5** The cycling stability of batteries with a PVDF-HFP+CNF interlayer, a PVDF-HFP interlayer and a CNF interlayer when the S loading is  $3.4 \text{ mg cm}^{-2}$ .

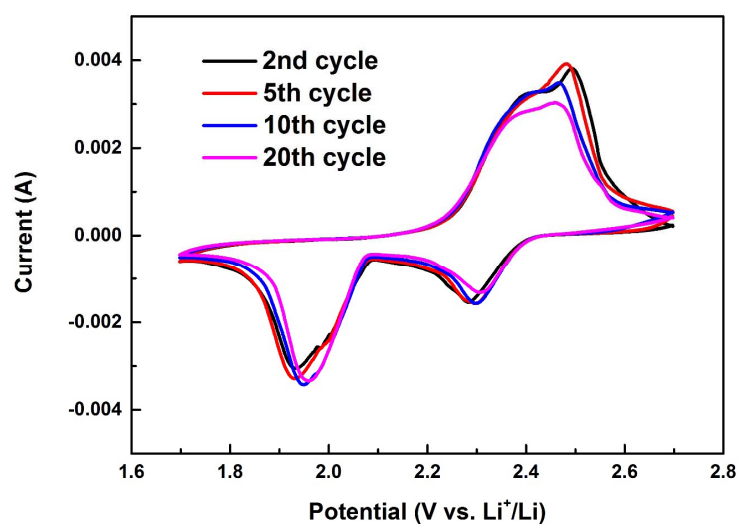


**Figure S6** The 2nd, 5th, 10th and 20th cycle CV curves of a battery with a PVDF-HFP+CNF interlayer.

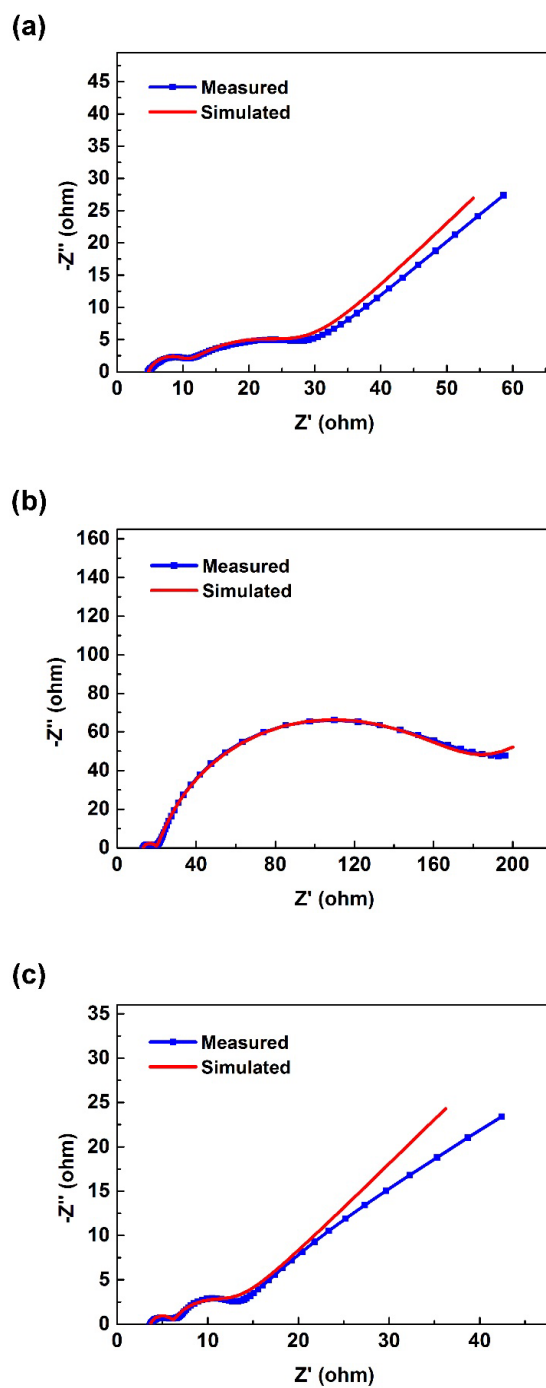


**Figure S7** Nyquist plots together with fitting curves of batteries with (a) a pristine CNF interlayer, (b) a pristine PVDF-HFP interlayer and (c) a PVDF-HFP+CNF interlayer after the 10th discharge process.

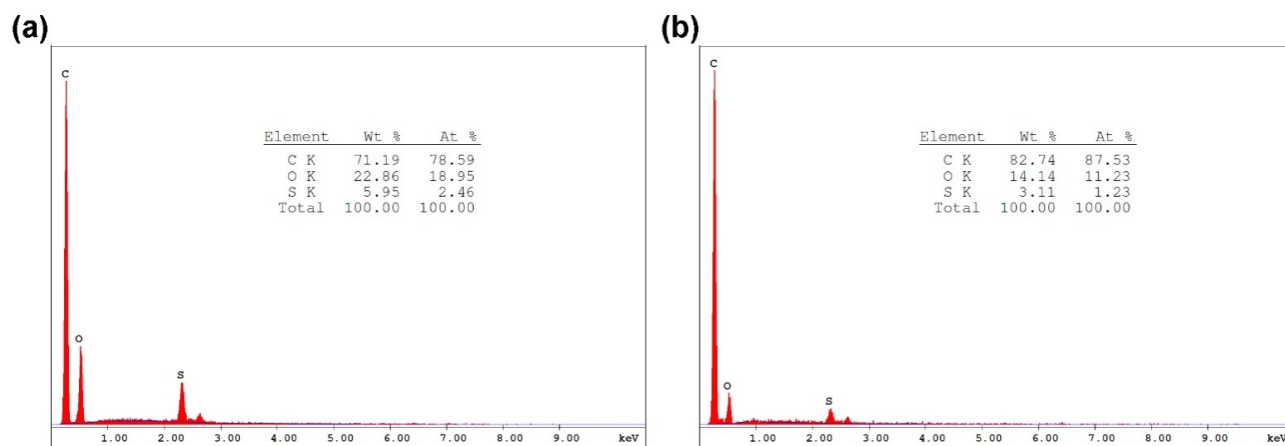


**Figure S8** EDX spectra on the surface of CNF S holder from batteries with (a) a pristine CNF interlayer and (b) a PVDF-HFP+CNF interlayer after the 10th discharge process.

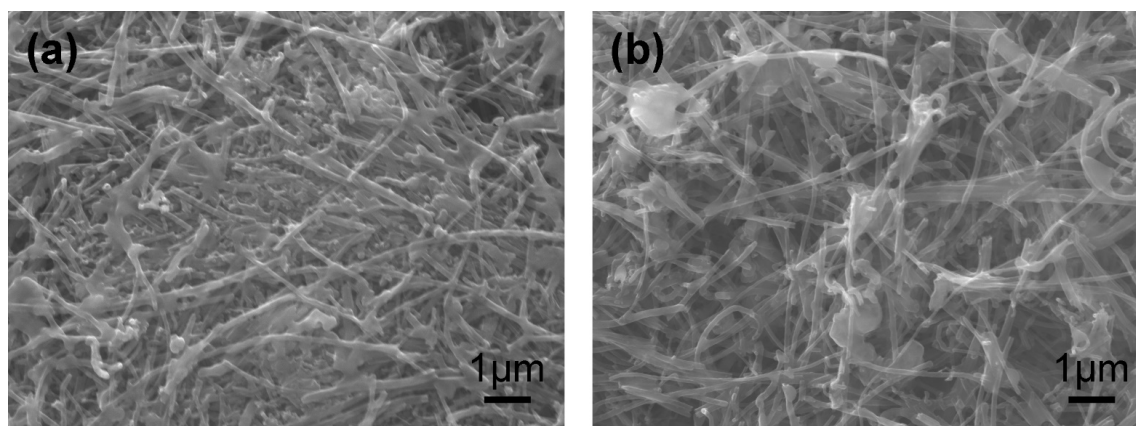


**Figure S9** SEM images on the surface of CNF S holder from cells with (a) a pristine CNF interlayer and (b) a PVDF-HFP+CNF interlayer after the 10th charge process.

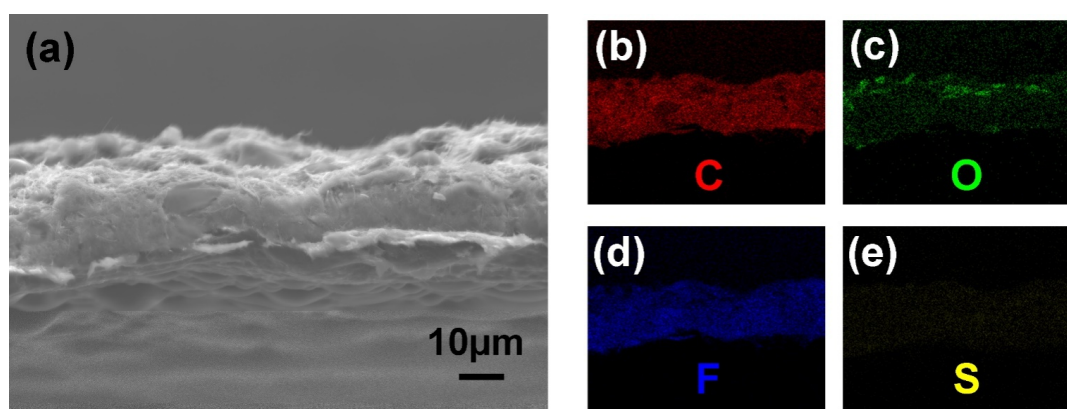


**Figure S10** (a) The cross-sectional SEM image and the corresponding EDX mapping images of (b) C, (c) O, (d) F and (e) S of a PVDF-HFP+CNF membrane after soaking in electrolyte and washing with DME twice.

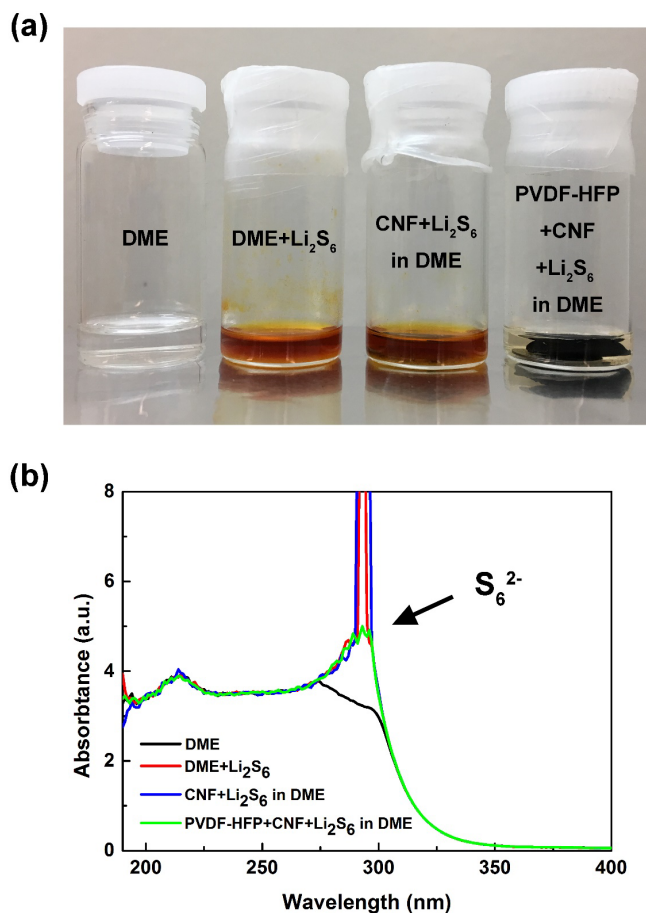


**Figure S11** A CNF and PVDF-HFP+CNF interlayers were dropped by Li<sub>2</sub>S<sub>6</sub> solution and submerged into DME to examine their absorption capability. (a) A photo and (b) UV-vis spectra were used to show the color difference qualitatively and quantitatively. The sample with PVDF-HFP absorbed more polysulfides and less Li<sub>2</sub>S<sub>6</sub> was detected in the DME solution, confirming the outstanding absorption capability.

## References:

- [1] Zheng, G.; Yang, Y.; Cha, J. J.; Hong, S. S.; Cui, Y. Hollow carbon nanofiber-encapsulated sulfur cathodes for high specific capacity rechargeable lithium batteries. *Nano Lett.* **2011**, *11*, 4462–4467.
- [2] Yang, J.; Xie, J.; Zhou, X.; Zou, Y.; Tang, J.; Wang, S.; Chen, F.; Wang, L. Functionalized N-Doped Porous Carbon Nanofiber Webs for a Lithium–Sulfur Battery with High Capacity and Rate Performance. *J. Phys. Chem. C* **2014**, *118*, 1800–1807.
- [3] Li, Q.; Zhang, Z.; Zhang, K.; Fang, J.; Lai, Y.; Li, J. A simple synthesis of hollow carbon nanofiber-sulfur composite via mixed-solvent process for lithium–sulfur batteries. *J. Power Sources* **2014**, *256*, 137–144.
- [4] Zheng, G.; Zhang, Q.; Cha, J. J.; Yang, Y.; Li, W.; Seh, Z. W.; Cui, Y. Amphiphilic surface modification of hollow carbon nanofibers for improved cycle life of lithium sulfur batteries. *Nano Lett.* **2013**, *13*, 1265–1270.
- [5] Yao, H.; Zheng, G.; Li, W.; McDowell, M. T.; Seh, Z.; Liu, N.; Lu, Z.; Cui, Y. Crab shells as sustainable templates from nature for nanostructured battery electrodes. *Nano Lett.* **2013**, *13*, 3385–3390.
- [6] Lu, S.; Cheng, Y.; Wu, X.; Liu, J. Significantly improved long-cycle stability in high-rate Li-S batteries enabled by coaxial graphene wrapping over sulfur-coated carbon nanofibers. *Nano Lett.* **2013**, *13*, 2485–2489.

